Journal of Materials Chemistry

Cite this: J. Mater. Chem., 2012, 22, 2520

www.rsc.org/materials

PAPER

A facile hydrazine-assisted hydrothermal method for the deposition of monodisperse SnO_2 nanoparticles onto graphene for lithium ion batteries†

Seung-Keun Park,‡[a] Seung-Ho Yu,‡[b] Nicola Pinna,[bc] Seunghee Woo,[d] Byungchul Jang,[a] Young-Hoon Chung,[b] Yong-Hun Cho,[e] Yung-Eun Sung*[b] and Yuanzhe Piao*[af]

Received 27th August 2011, Accepted 10th November 2011
DOI: 10.1039/c1jm14199f

In this manuscript, we introduce a facile hydrothermal method for the controlled growth of SnO_2 nanoparticles onto graphene oxide. Hydrazine plays a fundamental role in controlling the formation and crystallization of SnO_2 nanoparticles, and the reduction of graphene oxide to graphene. The SnO_2–graphene composite consists of 3–4 nm monodisperse SnO_2 nanocrystals homogeneously dispersed at the surface of graphene. It is demonstrated that the composite can accommodate the large volume change of SnO_2 which occurs during lithiation–delithiation cycles. When used as an anode material for lithium ion batteries, it exhibits a first discharge capacity of 1662 mA h g^{-1}, which rapidly stabilizes and still remains at 626 mA h g^{-1} even after 50 cycles, when cycled at a current density of 100 mA g^{-1}. Even at the very high current density of 3200 mA g^{-1}, the composite displays a stable capacity of 383 mA h g^{-1} after 50 cycles.

Introduction

Graphene, an atomic single layer of honeycomb carbon lattice, has attracted great attention recently because of its superior electronic conductivity, high surface area (theoretical value 2600 m^2 g^{-1}), and chemical and physical stability.[1,2] Since it was first reported in 2004, extensive research has been devoted to the fabrication of graphene-based nanostructures for energy storage,[3] sensing,[4] and composites.[5] However, because of the van der Waals interactions, unfunctionalized graphene sheets are prone to form irreversible agglomerates or restack to form graphite. Therefore, research on graphene based nanomaterials composites is focused on the reduction of the restacking, and stabilization with the aim to improve the performance.[6,7] Furthermore, graphene based nanomaterials composites can provide novel physical and chemical properties which can't be obtained from graphene itself. Especially, heterostructures composed of graphene and metal oxide nanoparticles are promising materials for electrodes in electrochemical devices.[8,9]

Among the metal oxides, tin oxide is an attractive material for the fabrication of negative electrodes for lithium ion batteries because of its high theoretical reversible capacity of 782 mA h g^{-1}, which is more than twice that of graphite.[10–18] Two electrochemical reactions take place in tin oxide based lithium ion batteries.[10,19]

$$SnO_2 + 4Li^+ + 4e^- \rightarrow Sn + 2Li_2O \quad (1)$$

$$Sn + xLi^+ + xe^- \leftrightarrow Li_xSn\ (0 \le x \le 4.4) \quad (2)$$

During the first cycle tin oxide is reduced to metallic tin following the irreversible reaction path (1). Further, lithiation produces a lithium–tin alloy *via* the reversible reaction (2). Unfortunately, in reaction (2) lithiation induces a large volume change, which causes cracking of the electrode and rapid degradation of the cycling performance. To solve these problems, various nanostructured SnO_2 and SnO_2 composites have been proposed with the aim of stabilizing the active electrode material by accommodating the volume change during cycling.[20,21] An improvement in the performances of the SnO_2/carbon nanocomposites was shown due to the role of the support which enabled a better accommodation of the large volume change and improved the electron conductivity of the electrode.[22,23] Graphene used as a substrate for metal oxide nanoparticles has already been shown to improve the mechanical stability and the

[a]*Department of Nano Science and Technology, Graduate School of Convergence Science and Technology, Seoul National University, Suwon, 443-270, Republic of Korea. E-mail: parkat9@snu.ac.kr; Fax: +82-31-8889148; Tel: +82-31-8889141*
[b]*World Class University (WCU) program of Chemical Convergence for Energy & Environment (C2E2), School of Chemical and Biological Engineering, College of Engineering, Seoul National University (SNU), Seoul, 151-744, Republic of Korea. E-mail: ysung@snu.ac.kr*
[c]*Department of Chemistry, CICECO, University of Aveiro, 3810-193 Aveiro, Portugal*
[d]*Department of Chemistry, Seoul National University, Seoul, 151-747, Republic of Korea*
[e]*School of Advanced Materials Engineering, Kookmin University, Seoul, 136-702, Republic of Korea*
[f]*Advanced Institutes of Convergence Technology, 864-1 Iui-dong, Yeongtong-gu, Suwon-si, Gyeonggi-do, 443-270, Republic of Korea*
† Electronic supplementary information (ESI) available. See DOI: 10.1039/c1jm14199f
‡ These authors contributed equally to this work

electrochemical performances.[24,25] Therefore, graphene–metal oxide composites are good candidates as anode materials for lithium ion batteries. Indeed, the application of these composites in rechargeable lithium ion batteries leading to enhanced performances has already been reported.[26–28] However, in previous reports, graphene–metal oxide composites were prepared in several steps before a final annealing aimed to improve the crystallinity of the oxide and to reduce the graphene oxide. Therefore, the known processes are commonly complicated and time-consuming.

In this paper, we introduce a novel one-pot process for the fabrication of SnO_2 nanoparticles–graphene nanocomposites based on hydrothermal synthesis assisted by hydrazine, which promotes the reduction of graphene oxide to graphene. This strategy provides a highly crystalline oxide and a more complete reduction of graphene oxide. Moreover, the composite exhibits outstanding cycling performance when used as an anode in lithium ion batteries.

Experiments

Preparation of graphene oxide

Graphene oxide (GO) was produced from graphite power (<20 micron) following Hummer's methods.[29] Briefly, 1 g of graphite, 1 g of $NaNO_3$ and 46 mL of H_2SO_4 were stirred together in an ice bath for 2 h. Then, 6 g of $KMnO_4$ were slowly added and reacted for 2 h. After the mixture was stirred vigorously for 5 days at room temperature, 250 mL of DI water was added. The solution was then slowly heated to 98 °C and maintained at this temperature for 1 h. 6 mL of H_2O_2 (30 wt%) were slowly added and the solution was filtered and washed with 1 : 10 HCl aqueous solution (250 mL) to remove metal ions followed by repeated washings with water and the solid was separated by centrifugation. Finally, the precipitate was dried at 70 °C overnight.

Preparation of graphene–SnO_2 composites

For the graphene–SnO_2 composites (GO–S) synthesis, 0.2 g of GO and 0.7 g (2 mmol) of $SnCl_4 \cdot 5H_2O$ were add to 60 mL of DI water followed by sonication for 30 min. Then, 485 μL of hydrazine monohydrate (80 wt%) were added to mineralize the tin ions. After 15 min of stirring, the mixture was transferred into a Teflon-lined stainless steel autoclave with a capacity of 100 mL and reacted under hydrothermal conditions at 160 °C for 12 h. The autoclave was slowly cooled down to room temperature, and a black-colored product was isolated by filtration and dried at 70 °C for 12 h.

Preparation of graphene nanosheets

Graphene nanosheets (GNS) were prepared by chemical reduction of GO. GO was dispersed in 100 mL of DI water (1 mg mL^{-1}) and this solution was reduced by heating at 100 °C for 2 h with hydrazine monohydrate (0.5 mL). The product was filtered and rinsed with DI water several times, and then dried.

Preparation of bare SnO_2 nanoparticles

For comparison, bare SnO_2 nanoparticles were prepared by a hydrothermal method. First, 1.4 g (4 mmol) of $SnCl_4 \cdot 5H_2O$ were added to 60 mL of DI water under stirring until a transparent solution was obtained. Next, 0.97 mL of hydrazine monohydrate (80 wt%) were added to the solution. After 15 min of stirring, the resulting slurry-like white solution was transferred into a Teflon-lined stainless steel autoclave and reacted at 160 °C for 12 h. Finally, a white-coloured product was isolated by centrifugation and dried at 70 °C overnight.

Characterization

X-ray photoelectron spectroscopy (XPS) experiments were performed in an UHV multipurpose surface analysis system (SIGMA PROBE, Thermo Fisher Scientific, UK) operating at base pressures $<10^{-10}$ mbar. The photoelectron spectra were excited by an Al Kα (1486.6 eV) anode operating at a constant power of 100 W (15 KV and 10 mA). The binding energies were shifted for charging by using C 1s to 284.6 eV as the reference. Fourier-transform IR (FT-IR) spectra were recorded using a Nicolet 6700 (Thermo Scientific, USA) in the infrared domain 400–4000 cm^{-1} with a KBr matrix. UV-vis absorption spectra were recorded using a PerkinElmer UV-Vis spectrometer Lamda 35. X-ray powder diffraction (XRD) patterns were obtained on a Bruker D-5005 with Cu K radiation ($\lambda = 1.5406$ Å) at 40 kV and 40 mA. For TGA measurements, a TA Instruments Q-5000 IR model was used with a heating rate of 5 °C min^{-1} in air. The morphology of our samples was characterized by scanning electron microscopy, SEM (Hitachi S-4800). A Tecnai F20 transmission electron microscope (TEM) equipped with a field emission gun and operated at 200 kV was used for high resolution TEM measurements.

Electrochemical measurement

Working electrodes were prepared from GO–S powder, Super P and poly(vinylidene fluoride) (70 : 15 : 15 in weight ratio) in *n*-methyl-2-pyrrolidinone. The slurry was coated onto a copper foil current collector *via* doctor blade processing and then pressed for use as the working electrode. The electrode was dried at 120 °C for 8 h. Electrochemical test cells were assembled in an argon-filled glove box using coin-type half-cells (2016 type) with lithium foil as a counter electrode. The organic electrolyte was composed of 1.0 M $LiPF_6$ in ethylene carbonate and diethyl carbonate (1 : 1 vol.%) The cells were galvanostatically charged and discharged in the voltage range from 2.0 to 0.01 V *vs.* Li/Li^+. Electrochemical measurements were made with a WBCS3000 cycler (WonA Tech, Korea) at room temperature.

Results and discussion

Fig. 1 shows the X-ray diffraction patterns of the GO–S, GNS, SnO_2 and GO. GO exhibits a sharp peak centered at $2\theta = 10°$, corresponding to an interlayer spacing of 0.85nm.[30] The characteristic peak of GO disappears in the GNS sample. On the other hand, the appearance of a broad peak centered at around $2\theta = 24°$, corresponding to diffraction from the (002) plane of graphite, proves that GO is indeed reduced during hydrazine

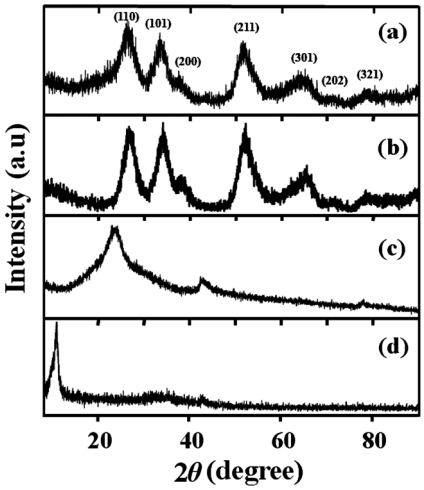

Fig. 1 XRD pattern of (a) GO–S, (b) bare SnO_2 (c) GNS and (d) GO.

treatment. This diffraction peak around 10° for GO was shifted to a higher angle of around 24°, indicating that GO was reassembled into GNS nanostacks. The XRD pattern of GO–S exhibits four major diffraction peaks (110), (101), (211), and (301), which are attributed to the tetragonal rutile SnO_2 phase (Cassiterite, JCPDS card No. 41-1445). These peaks are significantly broad, indicating a small particle size of SnO_2. The average crystallite size, determined from Scherrer's formula, was 3.5 nm. In the case of tin oxide, due to the overlapping of the main GNS reflection with the most intense 110 reflection of the cassiterite structure, its presence can be detected only because the latter become asymmetric. The large SnO_2 to graphene ratio was confirmed by TGA data (Fig. S1 in the ESI†) showing that 70 wt% of the sample is composed of SnO_2.

The morphology of the GNS and GO–S samples were studied by field emission scanning electron microscopy (FE-SEM) and TEM (Fig. 2). The SEM images revealed that the GNS has a wavy shape, consisting of various sheets arranged in a disordered manner(Fig. 2a). Although the morphology of GO–S composites also resembles that of GNS, the presence of tiny SnO_2 nanoparticles homogeneously distributed on the graphene are clearly observed (Fig. 2b,c). Also, the shape of graphene is crumpled paper-like and has many folded edges. On the other hand, the SnO_2 nanoparticles without GO are more aggregated than that of GO–S (Fig. S2 in the ESI†). These results show that the SnO_2 nanoparticles can be uniformly distributed on GO through the interaction between GO and SnO_2 nanoparticles.

High-resolution (HR) TEM images acquired from the edges of GO–S composites are presented in Fig. 3. The composites are formed by several graphene sheets stacked together with SnO_2 particles homogeneously dispersed at their surface (darker dots). In Fig. 3a and b the graphitic stack of graphene sheets is clearly visible (*cf.* arrows). The average particles size extracted from these images (~3–4 nm) is in good agreement with XRD data, suggesting that the nanoparticles should be single crystals. The power spectrum of a particle at the edge of the graphene sheets (Fig. 3a and inset) is characteristic of the SnO_2 Cassiterite structure for a particle oriented along the [001] direction. Similarly, Fig. 3b shows another region in which the multiple SnO_2 particles present well defined lattice fringes. As a peculiar

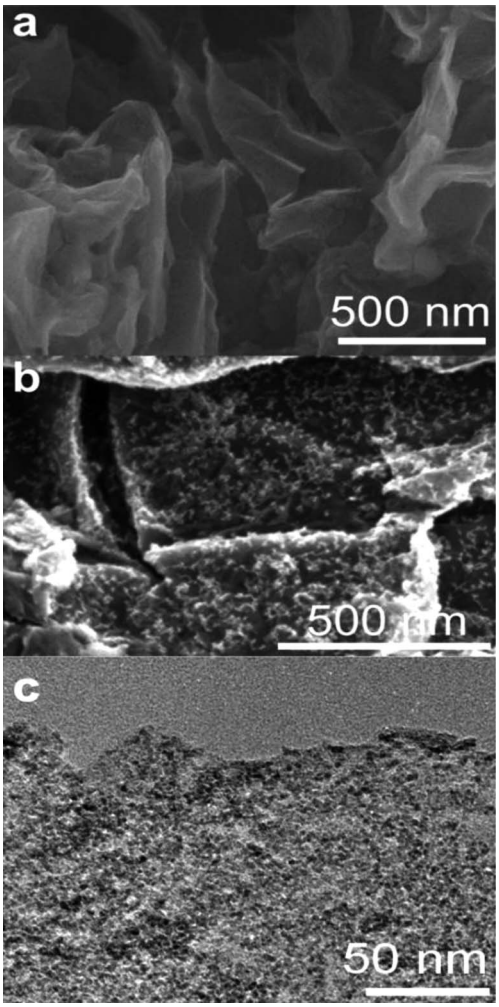

Fig. 2 SEM images of (a) GNS (b) GO–S and (c) TEM image of GO–S.

example, the power spectrum of the selected particles present three pairs of reflections characteristic of a single crystal imaged under the [111] zone axis.

In order to assess the reduction of graphene oxide, during the hydrothermal treatment assisted by hydrazine, Fourier transform infrared (FT-IR) spectra of the nanostructures were recorded (Fig. 4a). The FT-IR spectrum of GO shows the

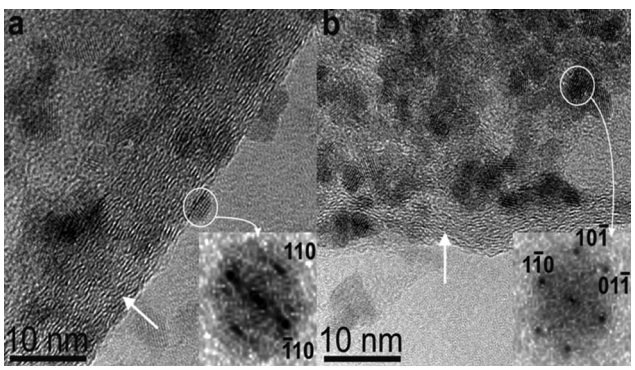

Fig. 3 HRTEM images of GO–S composites (insets: power spectra of the region indicated by a circle).

presence of various oxygen-containing groups, such as O–C=O ($\nu_{O-C=O}$ at 840 cm^{-1}), C–OH (ν_{C-OH} at 1220 cm^{-1}), O–H (ν_{O-H} at 1400 cm^{-1}) and carboxyl functional moieties at 1730 cm^{-1}, which are formed because of the strong oxidation process.[31] On the other hand, in the case of GNS and GO–S, most of the contributions due to oxygen-containing groups decrease after hydrothermal treatment, only the peak attributed to C–O centered at 1220 cm^{-1} still remains. It is known that the C–O groups can't be totally removed by chemical reduction methods.[32] However, these defects can help to control the growth of nanoparticles on graphene.[33] Furthermore, in the spectrum of GO–S, the remaining bands at 559 cm^{-1} and 670 cm^{-1} are assigned to the vibration of the Sn–OH terminal bonds and the anti-symmetric O–Sn–O stretching mode, respectively.[34]

Fig. 4b illustrates the UV-Vis absorption spectra of the three materials. The UV-Vis spectrum of GO exhibits two main peaks, one centered at 233 nm, corresponding to $\pi \rightarrow \pi^*$ transition of C=C bond, shifted to ~265 nm because of the reduction of GO and restoration of the conjugated aromatic system.[35] And a weak peak around 320 nm, representative of the $n \rightarrow \pi^*$ transition of the C=O bond. The latter disappears after hydrothermal treatment proving that the concentration of carboxyl groups decreases and that the GO is reduced during the synthesis of SnO_2.[36]

Chemical information was also obtained by XPS. The main signals present on the survey spectra of the GO and GNS are due to C and O, which are also the main components along with Sn in the GO–S (Fig. S3 in the ESI†). The binding energies of Sn $3d_{3/2}$ and Sn $3d_{5/2}$ are found at 487.7 eV and 496.1 eV, respectively, and are characteristic of Sn^{4+} (Fig. S4, in the ESI†).[37] The high-resolution C1s XPS spectrum is presented in Fig. 5. The C1s peak of graphene oxide consists of C–C (sp^2 carbon in the basal plane, 284.6 eV), C–O (286.5 eV), C=O (288.1 eV) and O–C=O (289 eV).[38] The contribution of C–O is particularly high. After hydrothermal treatment, the O/C ratio decreases notably in GNS and GO–S, suggesting that the large majority of the oxygenated species are removed. In addition, a C–N (285.1 eV) bond was observed after hydrazine reaction. Finally, a broad and weak peak centered above 290.0 eV is identified as a shake-up satellite due to π–π^* transitions.

The GO–S was prepared by chemical deposition of tin ions onto the GO sheets. The abundant functional groups (epoxy-, hydroxyl-, carboxyl-), presumed to be uniformly distributed on the surface of the GO sheets,[32] can act as anchoring sites for tin ions through electrostatic attraction. One can therefore assume

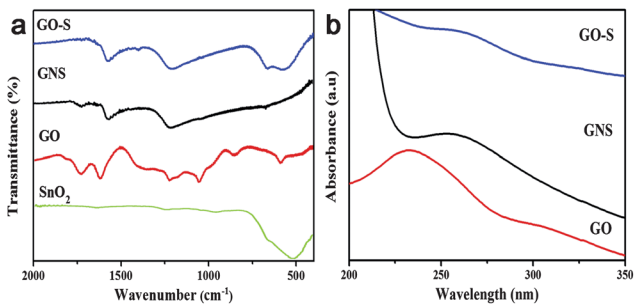

Fig. 4 (a) FT-IR spectra of GO–S, GNS, GO and SnO_2, (b) UV-vis spectra of GO–S, GNS and GO.

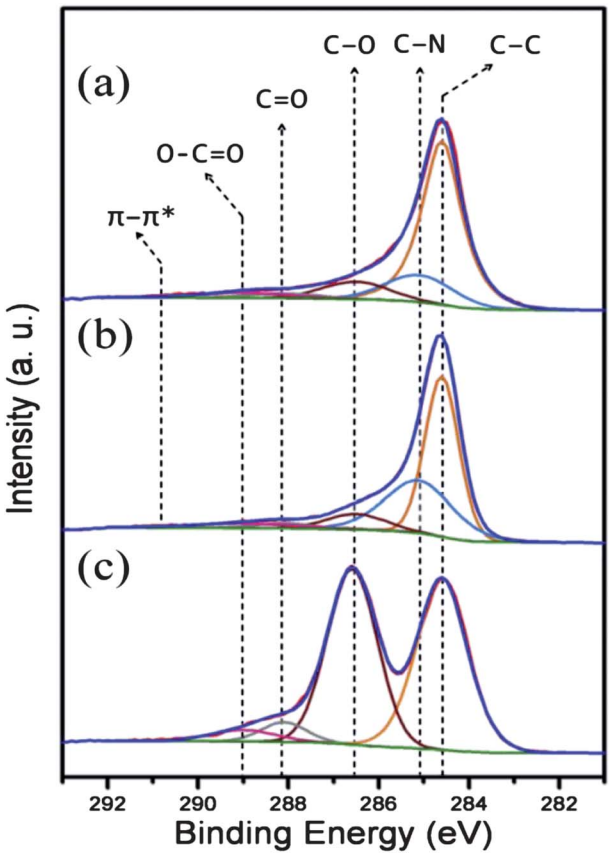

Fig. 5 XPS spectra: high-resolution C 1s of (a) GO–S, (b) GNS and (c) GO.

that the oxygenated groups coordinate the Sn^{4+} and act as a nucleation center for the SnO_2 nanoparticles growth. It enables the deposition of a uniform nanoparticle film to uniformly distribute on graphene through interaction with graphene. Instead of the most commonly used NaOH or NH_3,[39,40] in this work hydrazine plays the role of mineralizer. Furthermore, it promotes SnO_2 nanoparticles formation *via* $(SnCl_4)_m(N_2H_4)_n$ complexes, which are formed as soon as hydrazine is added to the reaction mixture.[41] These complexes, composed of bridging H_2N–NH_2, are the intermediate species governing the formation of the SnO_2 nanoparticles, which takes place under hydrothermal conditions *via* their thermal decomposition. As a result, 3–4 nm SnO_2 nanoparticles on graphene were obtained through the hydrothermal process. On the other hand, it is known that small-sized SnO_2 are difficult to obtain by using NH_4OH as the mineralizer under hydrothermal conditions.[42] Thus, our method was expected to improve electrochemical properties due to the smaller particle size. In addition, hydrazine acts as a reducing agent of GO as demonstrated above.

The electrochemical performances of the GO–S were evaluated by galvanostatic charge–discharge cycling between 10 mV and 2 V at a current density of 100 mA g^{-1} (Fig. 6a). In the first cycle, GO–S electrode material delivered a discharge capacity of 1662 mA h g^{-1} and a charge capacity of 819 mA h g^{-1}. The coulombic efficiency at the first cycle is low (around 49%) due to the irreversible formation of amorphous lithium oxide and a solid electrolyte interface layer (SEI). During the initial cycles,

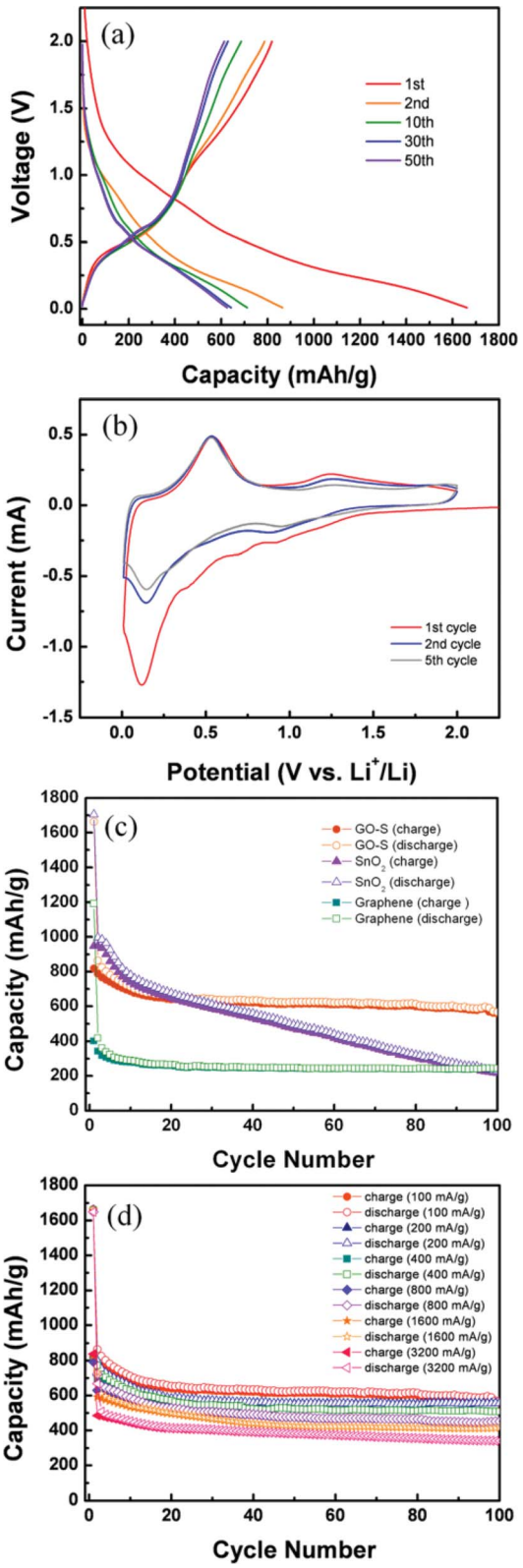

Fig. 6 (a) The charge–discharge curves of GO–S at a current density of 100 mA g^{-1}, (b) cyclic voltammograms of the GO–S at a scanning rate of 0.1 mV s^{-1}, (c) cycling performance of GO–S, SnO_2 and graphene at a current density of 100 mA g^{-1}, (d) cycling performance of GO–S at various current densities after 1 cycle at a current density of 100 mA g^{-1}.

the specific capacity decreases, before stabilizing after 20 cycles. In order to better understand the reaction mechanism cyclic voltammetry was performed (Fig. 6b). In the first cycle, the weak irreversible cathodic peak at around 0.74 V is attributed to the formation of the solid electrolyte interface layer. This peak is not present in the second cycle and onwards. The clear cathodic peak around 0.12 V and the anodic peak around 0.54 V are related to the lithium alloying reaction with Sn and de-alloying of Li_xSn, respectively. Also, the reduction peak at about 0.01 V and the oxidation peak at about 0.1 V correspond to the lithium insertion and extraction from the graphene sheets.

Fig. 6c shows the cycling performance of the GO–S, pure SnO_2 nanoparticles and graphene, respectively. The capacity of pure SnO_2 decreases continuously due to the large volume change during the cycling, resulting in the aggregation of Sn. On the other hand, tin nanoparticles on graphene are less likely to aggregate into larger clusters than tin particles without graphene during cycling, which is confirmed by TEM. (Fig. S5 in the ESI†). Fig. 6d presents the cycling performance of GO–S evaluated at various current densities for up to 100 cycles. It is evident that the graphene framework has greatly improved the electron transfer and the stability of the electrode compared to pure SnO_2. Even at a current density of 3200 mA g^{-1}, GO–S delivered a high capacity of 380 mA h g^{-1} after 50 cycles, which is higher than the theoretical capacity of graphite (372 mA h g^{-1}).

Conclusions

In summary, a facile one-pot synthesis approach was developed for the controlled deposition of SnO_2 nanoparticles on graphene. During the reaction, monodispersed SnO_2 nanoparticles are formed on graphene because of the formation of an heteroleptic complex between Sn ions and hydrazine. The high crystallinity of the as-synthesized SnO_2 nanoparticles is clearly one of the peculiarities of the approach. The graphene–SnO_2 composite was used as an anode material for lithium ion batteries. It showed stable cycling performance and higher capacity than the SnO_2 and graphene due to the stabilization roles of graphene. Therefore, the results presented in this manuscript prove that graphene-based heterostructures synthesized by this novel hydrothermal method are good candidates for use as anode materials in lithium ion batteries. Finally, this synthesis approach can be probably extended and generalized to a large variety of metal oxides.

Acknowledgements

This research was supported by the Basic Science Research Program through the National Research Foundation of Korea (NRF) funded by the Ministry of Education, Science and Technology (No. 2011-0025391) and partial support from the Korea Research Council of Fundamental Science and Technology (KRCF) through the project of 'Development of Characterization Techniques for Nano-materials Safety'. YES acknowledges financial support from the National Research Foundation of Korea Grant funded by the Korean Government (MEST) (NRF-C1AAA001-2010-0029065). Yong-Hun Cho acknowledges financial support by the Priority Research Centers Program through NRF funded by MEST (2009-0093814).

References

1 K. S. Novoselov, A. K. Geim, S. V. Morozov, D. Jiang, Y. Zhang, S. V. Dubonos, G.I. V. and A. A. Firsov, *Science*, 2004, **306**, 666.
2 A. K. Geim, K. S. Novoselov, S. V. Morozov, D. Jiang, M. I. Katsnelson, I. V. Grigorieva, S. V. Dubonos and A. A. Firsov, *Nature*, 2005, **438**, 197.
3 E. Yoo, J. Kim, E. Hosono, H. Zhou, T. Kudo and I. Honma, *Nano Lett.*, 2008, **8**, 2277.
4 J. F. Wu, M. Q. Xu and G. C. Zhao, *Electrochem. Commun.*, 2010, **12**, 175.
5 S. Stankovich, D. A. Dikin, G. H. B. Dommett, K. M. Kohlhaas, E. J. Zimney, E. A. Stach, R. D. Piner, S. T. Nguyen and R. S. Ruoff, *Nature*, 2006, **442**, 282.
6 S. Stankovich, R. D. Piner, X. Q. Chen, N. Q. Wu, S. T. Nguyen and R. S. Ruoff, *J. Mater. Chem.*, 2006, **16**, 155.
7 C. Xu, X. Wang and J. W. Zhu, *J. Phys. Chem. C*, 2008, **112**, 19841.
8 K. B. Kim, H. K. Kim and S. M. Bak, *Electrochem. Commun.*, 2010, **12**, 1768.
9 H. Q. Cao, B. J. Li, J. Shao, M. Z. Qu and J. H. Warner, *J. Mater. Chem.*, 2011, **21**, 5069.
10 I. A. Courtney and J. R. Dahn, *J. Electrochem. Soc.*, 1997, **144**, 2045.
11 T. Brousse, R. Retoux, U. Herterich and D. M. Schleich, *J. Electrochem. Soc.*, 1998, **145**, 1.
12 N. C. Li, C. R. Martin and B. Scrosati, *Electrochem. Solid-State Lett.*, 1999, **3**, 316.
13 N. C. Li and C. R. Martin, *J. Electrochem. Soc.*, 2001, **148**, A164.
14 C. Kim, M. Noh, M. Choi, J. Cho and B. Park, *Chem. Mater.*, 2005, **17**, 3297.
15 X. W. Lou, Y. Wang, C. L. Yuan, J. Y. Lee and L. A. Archer, *Adv. Mater.*, 2006, **18**, 2325.
16 H. Kim and J. Cho, *J. Mater. Chem.*, 2008, **18**, 771.
17 X. W. Lou, D. Deng, J. Y. Lee and L. A. Archer, *Chem. Mater.*, 2008, **20**, 6562.
18 J. Y. Huang, L. Zhong, C. M. Wang, J. P. Sullivan, W. Xu, L. Q. Zhang, S. X. Mao, N. S. Hudak, X. H. Liu, A. Subramanian, H. Y. Fan, L. A. Qi, A. Kushima and J. Li, *Science*, 2010, **330**, 1515.
19 X. Wang, X. Zhou, K. Yao, J. Zhang and Z. Liu, *Carbon*, 2011, **49**, 133.
20 M.-S. Park, Y.-M. Kang, G.-X. Wang, S.-X. Dou and H.-K. Liu, *Adv. Funct. Mater.*, 2008, **18**, 455.
21 S. J. Han, B. C. Jang, T. Kim, S. M. Oh and T. Hyeon, *Adv. Funct. Mater.*, 2005, **15**, 1845.
22 X. W. Lou, J. S. Chen, P. Chen and L. A. Archer, *Chem. Mater.*, 2009, **21**, 2868.
23 M. S. Park, Y. M. Kang, J. H. Kim, G. X. Wang, S. X. Dou and H. K. Liu, *Carbon*, 2008, **46**, 35.
24 J. W. Zhu, S. Chen, X. D. Wu, Q. F. Han and X. Wang, *ACS Nano*, 2010, **4**, 2822.
25 R. S. Ruoff, Y. W. Zhu, S. Murali, M. D. Stoller, K. J. Ganesh, W. W. Cai, P. J. Ferreira, A. Pirkle, R. M. Wallace, K. A. Cychosz, M. Thommes, D. Su and E. A. Stach, *Science*, 2011, **332**, 1537.
26 H. H. Wang, P. C. Lian, X. F. Zhu, H. F. Xiang, Z. Li and W. S. Yang, *Electrochim. Acta*, 2010, **56**, 834.
27 J. Z. Wang, C. Zhong, D. Wexler, N. H. Idris, Z. X. Wang, L. Q. Chen and H. K. Liu, *Chem.–Eur. J.*, 2011, **17**, 661.
28 X. Zhu, Y. Zhu, S. Murali, M. D. Stoller and R. S. Ruoff, *J. Power Sources*, 2011, **196**, 6473.
29 W. S. Hummers and R. E. Offeman, *J. Am. Chem. Soc.*, 1958, **80**, 1339.
30 Y. M. Li, X. J. Lv, J. Lu and J. H. Li, *J. Phys. Chem. C*, 2010, **114**, 21770.
31 R. Bissessur, P. K. Y. Liu, W. White and S. F. Scully, *Langmuir*, 2006, **22**, 1729.
32 D. Li, M. B. Muller, S. Gilje, R. B. Kaner and G. G. Wallace, *Nat. Nanotechnol.*, 2008, **3**, 101.
33 H. L. Wang, J. T. Robinson, G. Diankov and H. J. Dai, *J. Am. Chem. Soc.*, 2010, **132**, 3270.
34 S. M. Paek, E. Yoo and I. Honma, *Nano Lett.*, 2009, **9**, 72.
35 H. L. Wang, L. F. Cui, Y. A. Yang, H. S. Casalongue, J. T. Robinson, Y. Y. Liang, Y. Cui and H. J. Dai, *J. Am. Chem. Soc.*, 2010, **132**, 13978.
36 G. Eda, Y. Y. Lin, C. Mattevi, H. Yamaguchi, H. A. Chen, I. S. Chen, C. W. Chen and M. Chhowalla, *Adv. Mater.*, 2010, **22**, 505.
37 P. G. Li, X. Guo, X. F. Wang and W. H. Tang, *J. Alloys Compd.*, 2009, **479**, 74.
38 C. S. Ha, V. K. Rana, M. C. Choi, J. Y. Kong, G. Y. Kim, M. J. Kim, S. H. Kim, S. Mishra and R. P. Singh, *Macromol. Mater. Eng.*, 2011, **296**, 131.
39 H. B. Yang, J. Xu, Q. J. Yu, L. X. Chang, X. F. Pang, X. Li, H. Y. Zhu, M. H. Li and G. T. Zou, *Mater. Lett.*, 2007, **61**, 1424.
40 G. V. Lysak, I. A. Lysak, T. D. Malinovskaya and G. G. Volokitin, *Inorg. Mater.*, 2010, **46**, 183.
41 H. L. Zhu, D. R. Yang, G. X. Yu, H. Zhang and K. H. Yao, *Nanotechnology*, 2006, **17**, 2386.
42 H. N. Lim, R. Nurzulaikha, I. Harrison, S. S. Lim, W. T. Tan and M. C. Yeo, *Int. J. Electrochem. Sci.*, 2011, **6**, 4329.